Low-Gravity Effects During Solidification

By Peter A. Curreri
Materials Scientist
NASA, Marshall Space Flight Center

and

Doru M. Stefanescu
Professor of Metallurgy
University of Alabama

Solidification processes are strongly influenced by gravitational acceleration through Stokes flow, hydrostatic pressure, and buoyancy driven thermal and solutal convection. Stokes flow of second phase particles in off-eutectic and off-monotectic alloys, and non-contiguous metal matrix composites severely limits casting composition. Porosity in equiaxed casting is dependent on hydrostatic pressure. Convective flow can dominate heat and mass transfer in the liquid ahead of the solid/melt interface.

Buoyancy independent solidification within the gravitational field at the earth's surface is accomplished only within strict limits. In one dimension, strong magnetic fields can dampen convection, and density gradients can be oriented with gravity for stability. But, magnetic flow dampening in one direction increases flow velocity (segregation, etc.) in the transverse direction. Opposition of thermal and solutal convection for many alloy compositions make stabilization of convection by orientation, even in one dimension, unfeasible.

Space flight provides solidification research the first long duration access to micro-gravity. Supporting commercial and academic interest in solidification in Space are several short duration free fall facilities. These include: drop towers (4 sec., 0.0001 g, g=980 cm./sec.^{2}), parabolic aircraft flight (30 sec., 0.01 g; 1 min., 1.8 g repetitive cycles), and sub-orbital sounding rockets (5 min., 0.0001 g).

Convection and the Melt Temperature Field

<u>Thermal Convection and G_L</u>. Solidification progresses through the melt as a result of extraction of heat from the liquid at the solid/melt interface. Thermal gradients during solidification are thus present in the melt causing density gradients that under a gravitational field result in buoyancy driven convective flows. Convective flow, for constant furnace conditions, can modify the liquid thermal gradient at the solid/liquid interface, G_L.

The sensitivity of the melt thermal profile to convection is

strongly a function of liquid physical properties. A dimensionless number from the Navier-Stokes equations useful in determining the sensitivity of a melt thermal profile in response to convective flow is the Prandtl Number, Pr. Pr is defined by

$$Pr = \mu C_p / k \qquad [1]$$

where μ is viscosity (kg/m^2), C_p is specific heat (J/g.K), and k is thermal conductivity (W/m.K). At low Pr the convective transport of momentum dominates the convective transfer of heat, thus, thermal convection has less influence on the temperature field. Pr for liquid metals is generally much less than one (on the order of Pr = 0.01). Ammonium chloride/water melts (often used as transparent analogs for metal solidification) have Pr = 6. The response of the temperature fields to fluid flow is given schematically in Figure 1 for high and low Pr.

Since alloy microstructure and solid/liquid interface morphology, for a given composition and growth velocity, is dependent on G_L, the influence of convection on the liquid thermal profile has been extensively modeled. One configuration examined is unidirectional solidification in the vertically stabilized configuration - solidification antiparallel to gravity (less dense hotter fluid upward). Temperature field numerical results (2) for Ga doped Ge (Pr = 0.01) show that the thermal isotherms in the melt at the crucible center line compress (higher G_L) at high gravity due to convective flow. The thermal gradient at the crucible wall decreases with higher convection. This results from convective flow of hot liquid towards the crystal/melt interface center that is compensated for by flow of cold liquid away from the solidification interface at the crucible walls. Thus, under strong convection the minimum G_L across the solid/liquid interface increases in the absence of thermal convection, implying for example, a decrease in interfacial morphological stability in low gravity.

Solutal Convection and G_L. At the growing interface during alloy solidification solute often is rejected of differing density from the bulk liquid. Under a gravitational field (even if the system is stable for thermal convection) this results in solutal convection. Thermal and solutal density gradients combine to cause "thermosolutal convection." For metal alloys the solute expansion coefficient is normally large compared to the thermal expansion coefficient causing solutal convective flow to dominate.

Laser interferograms of solidifying ammonium chloride given in Figure 2 illustrate the development of solutal convection. When the ampule of ammonium chloride is placed on a cold block solidification begins upward. Growth enriches in solute the liquid ahead of the solid/liquid interface decreasing its density relative to the bulk melt. The solute rich layer builds up until a plume of less dense solute breaks away from the interface and travels upward in the melt. The solutally driven convective flow decreases the liquid thermal gradient at the solid/liquid interface. The effect on the temperature field is amplified by

the system's high Pr (Pr = 6). The experiment was repeated in in low gravity during aircraft parabolic flight ($g = 10^{-2}$). G_L in low gravity (relative to G_L in one gravity) counter to what would be expected from thermal convection alone, was 15% greater.

Low gravity experiments with metallic alloys (low Pr), as expected from Figure 1, find less dependence of G_L on convective flow. Thermal-couple measurements for three directionally solidified eutectic Mn/MnBi samples on the Space Processing Applications Rocket Project, SPAR IV, sounding rocket ($g = 10^{-4}$) flight, for example, found G_L to be statistically equivalent with samples solidified in one gravity.

Convection and Solute Redistribution, Plain Front Solidification

The solute concentration in the solid during alloy solidification differs (unless the partition coefficient is one) from that in the liquid ahead of the solidification interface. When the liquid ahead of the solidification interface is continually well mixed by convective flow the resulting solute concentration in the solid (if diffusion in the solid is negligible) continually increases. If instead the solute rejected into the liquid is transported only by diffusion, a solute enriched boundary layer forms in the liquid ahead of the solid/liquid interface and increases in solute concentration as solidification progresses until a steady state is reached. Alloy solidification in the prescience of a steady state boundary layer can, in contrast to the example with strong convection, solidify with a nearly constant composition. Low gravity planar growth experiments with Te doped In-Sb (Skylab, 1972) first demonstrated improved crystal solute homogeneity (over that for growth in one gravity) by steady state diffusion boundary layer controlled growth.

Stagnant Film Models. Variable thickness diffusion boundary layer (Stagnant film) models are often used to assess the influence of convective flow on the solute distribution during solidification. Convective flow is assumed to completely mix the solute in the melt outside the diffusion boundary layer. The boundary layer thickness decreases with increasing convective flow. Inside the diffusion boundary layer the model assumes solute transport is by diffusion only. For intermediate convective flow velocity the model assumes a dynamic diffusion boundary layer that yields a constant solid composition defined by an effective (convective dependent) partition ratio. At high convective flow the boundary layer approaches zero yielding a solid solute concentration that varies with solidified fraction.

Stagnant film models are often used in the literature for simplicity of calculation. The assumption that convective flow does not penetrate the diffusion boundary layer, however, leads to incorrect predictions. The transverse diffusion boundary layers for on-eutectic growth or secondary dendrite arms are much smaller than the momentum boundary layer that the model considers is affected by convective flow. Stagnant film models, thus,

falsely predict that even vigorous convective flow will have no effect for on-eutectic or secondary dendritic spacings.

Numerical Solution of Solute Redistribution. Finite element methods more accurately model convective flow at the melt/solid interface and the resulting solute segregation. Numerical predictions (2) are qualitatively similar to those of the Stagnant film models. However, finite element calculations reveal that a stagnant boundary layer does not exist in the presence of convection. Flow within the "diffusion boundary layer" has a strong convective flow contribution. This contribution must be carefully considered in analyzing the effect of convection on microstructure.

Solidification of Composites in Low Gravity

Eutectic Alloys. Buoyancy driven convective and Stokes flow strongly affect eutectic solidification. Casting of off-eutectic alloys with independently nucleated primary phase (under normal gravity) results in severe macrosegregation due to Stokes flow. An example is kishing of graphite in castings of hypereutectic gray iron. Solidification in zero gravity eliminates Stokes flow. Low-gravity experiments with off-eutectic iron-carbon alloys (4) have shown that primary graphite flakes or nodules that float away from the interface in normal gravity are incorporated into the solidifying interface under low gravity. Thus, solidification of off-eutectic castings with independently nucleated primary particles in zero gravity eliminates macrosegregation due to Stokes flow.

Cooperative growth of on-eutectic alloy has been shown to be strongly influenced by convection. On-eutectic MnBi/Bi was solidified in low gravity on Space Processing Applications (sounding) Rocket flights, SPAR VI (R=6 mm./min.) and SPAR IX (8.3 mm./min.) (5). Sample microstructure, composition, and properties were compared to 1 gravity controls (solidified under identical conditions except for gravity). The eutectic interphase spacing (relative to 1 g controls) for low-gravity solidified sample decreases by over 50 %. This is evident in the transverse sections given in Figure 3. A decrease in rod diameter is also apparent in for low-gravity solidified sample. Volume fraction of MnBi rods in low gravity samples is also smaller (about 7%). Thermal data reveals increased interfacial undercooling (3-5 C) during low-gravity solidification. Low gravity solidification produced samples (Figure 4) with increased intrinsic coercivity (resistance to demagnetization).

Phase spacing refinement can of course also be achieved in one gravity by increasing solidification rate, R. Figure 5 gives the interrod spacings, lambda, as a function of R under various processing conditions. It is evident (Figure 5) that orientation of sample in one gravity has no effect on interrod spacing. At higher R the spacing appears to obey lambda R^2 = constant, with the exception of finer spacing for low-gravity samples.

Table I includes these first results and data reported from subsequent studies (7). Interphase spacing refinement during low-gravity solidification is observed for both Fibrous (MnBi/Bi and InSb/NiSb) and lamellar (Fe_3C/Fe) on-eutectic compositions. Gravity independence of lamellar spacing is reported for Al-Cu and an decrease in spacing for low gravity is reported for Al_3Ni/Al. Although results for each alloy prove reproducible, there is no obvious trend.

The mechanism for low gravity's influence during on-eutectic solidification on phase spacing is yet to be established. Convective flow's importance is demonstrated, for MnBi/Bi, by the duplication of low gravity spacing and interfacial undercooling through solidification in strong (3 kG) magnetic fields. The effect of gravity on convective flow is relatively well understood. The challenge is to develop a theory adequately relating convective flow at low gravity to the mechanisms controlling eutectic phase spacing. Several approaches being pursued to develop the needed theory are listed below in relation to experimental findings.

(a) Analysis of Convective Flow for On-Eutectic Growth

Simple stagnant film model predicts that cooperative on-eutectic growth will be unaffected by the presence (or absence) of convection. Solute redistribution for on-eutectic growth occurs on the scale of the lamellar spacing, which is much smaller then the convective flow momentum boundary layer (on the order of D/R). Thus, for steady state on-eutectic growth at fixed volume fraction convective flow is not expected to affect lamellar spacing.

More rigorous analysis (8) demonstrates invalidity in the above conclusions. The actual flow fields (diffusive and convective) in the liquid ahead of the eutectic solid-liquid interface are numerically calculated. A series of curves for lamellar spacing versus interfacial undercooling for a given R (Figure 6) can be determined for different magnitudes of forced convective flow. Growth is assumed to be preferred at the "extremum" (minimum interfacial undercooling) which then defines the eutectic spacing for a given R.

The theory predicts forced convection decreases interfacial undercooling and increases interphase spacing. The theory semiquantitatively predicts phase spacing at high convective flows for Ti/Ti_5Si_3, MnBi/Bi, and Fe/Fe_2Bi. Qualitatively, the theory predicts the low-gravity results for MnBi/Bi eutectic (Table I).

When the theory is applied (9) to MnBi/Bi low-gravity solidification data, the calculated disturbance in the eutectic diffusion field at one gravity is so slight that the calculated eutectic phase spacing for solidification in one gravity or in Space are essentially equivalent. Thus, the calculated effect of convective flow on the liquid concentration field does not

explain the low-gravity eutectic lamellar spacings.

(b) Off-Eutectic Approach

Other researchers (7) propose off-eutectic models to account for the influence of low gravity on eutectic spacing. They postulate an arbitrary 1% deviation from eutectic composition. Boundary layer theory is used to predict the effect of convection on the volume fraction term in the equations for eutectic spacing.

Off-eutectic models offer several advantages. The solute redistribution boundary layer is on the order of D/R - much larger than that (eutectic spacing, λ) for on-eutectic cooperative growth. Convection has a much more pronounced effect on the concentration field ahead of the solid-liquid interface. The sign of the composition deviation from eutectic determines the sign of the low-gravity induced phase spacing change - low-gravity spacing that are smaller for hypereutectic and larger for hypoeutectic. No change, insensitivity to convection, is also predicted for some materials.

MnBi/Bi eutectic samples experience considerable solid-liquid interfacial undercooling during directional solidification in low gravity. Under equivalent solidification conditions except in one gravity MnBi/Mn essentially solidifies at the eutectic temperature. Volume fraction, f_v, MnBi data (Figure 7) for MnBi/Bi show on-eutectic type solidification in normal gravity and Bi rich off-eutectic type solidification in low-gravity.

It is not known, due to lack of published data, if the other alloys in Table I also experience increased eutectic solid-liquid interfacing undercooling in low gravity. Alloy dependent undercooling in low gravity could explain the data in Table II.

The off-eutectic model tested (7) with the f_v flight data for MnBi/Bi (Figure 7) obtains $\lambda_{R1g} = 1.05\ \lambda_{R0g}$. This is only 10% of the observed change. Thus, the gravity dependent change in f_v, using the Jackson and Hunt type expression, can only partially explain low-gravity eutectic spacings.

(c) Diffusion / Atomic Transport

Neither on-eutectic nor off-eutectic convection models predicts the data in Table I. Convective effects on thermal gradient and growth rate also fail to explain the low-gravity eutectic spacing.

Another approach (7) examines gravity's influence on solidification through microconvections driven by microscopic concentration and temperature gradients or by thermodynamic liquid density fluctuations. These microconvections are independent of the previously discussed macroconvection but are indistinguishable from collective atomic motion - liquid diffusion. The effective liquid diffusion coefficient, D_{eff}, in

normal gravity consists of the intrinsic diffusion coefficient plus an atomic transport component due to microconvection. Low-gravity liquid metal diffusion experiments for Zn and Sn (7) find $D_{eff}(0g)$ is less than $D_{eff}(1g)$ by 10-60%. A decrease in D_{eff} of this order could explain (7) in the magnitude of lamellar spacing decrease found for low-gravity solidified Fe/Fe_3C and Bi/MnBi. The low-gravity data for on-eutectic spacing for Al-Cu and Al_3Ni/Al, however, have yet to be convincingly explained by this approach.

Monotectic Alloys. Monotectic alloys contain a miscibility gap or dome in their phase diagram. During off-monotectic alloy solidification in the temperature region through the miscibility gap two immiscible liquids exist in equilibrium. Melt processing in normal gravity results in density driven Stokes coalescence of the liquid droplets and massive segregation similar to that experienced for oil and water type dispersions. Powder metallurgical methods are thus used to prepare hypermonotectic compositions. However, the interfacial purity necessary to exploit advanced technological electronic properties applications of hypermonotectic alloys is difficult to maintain with powder metallurgical processing. Off-monotectic alloys have thus had only limited technical importance.

Low gravity drop-tower experiments with Ga-Bi demonstrated the feasibility of producing high volume fraction immiscible alloys with finely dispersed microstructure (Figure 8) by low gravity solidification. Subsequent low-gravity experiments have identified a number of non-buoyancy driven coalescence mechanisms. Surface wetting of the crucible by the minority liquid, thermal migration of droplets, interfacial energies difference between the liquid phases and solid, surface tension driven convection, and nucleation kinetics must all be carefully controlled to obtain fine dispersions of hypermonotectic alloys in low gravity.

Hypermonotectic solidification in low gravity has often resulted (relative to sample solidified in one gravity) in samples with enhanced electronic properties. Low-gravity solidified Ga-Bi samples exhibit unusual resistivity versus temperature characteristics (Figure 9) and possess a superconducting phase with a higher transition temperature, T_c, (Figure 10). Skylab experiments for Pb-Sb-Zn and Au-Ge hypermonotectic alloys also report a phase with higher T_c (than that of one-gravity control samples) for sample solidified in low gravity. Al-In-Sn hypermonotectic alloy directionally solidified during low-gravity parabolic maneuvers also yield a higher T_c minority phase present only in low-gravity sections. The low-gravity sections exhibit semi-metal temperature versus resistance characteristics while the one and high-gravity sections are metallic (Figure 11).

Metal Matrix Ceramic Composites. Melt processing of ceramic metal composites, although less commonly employed than powder metallurgy, has some important advantages. These include

better matrix particle bonding, control of the matrix solidification, and processing simplicity. Melt processing is, however, severely limited by gravity driven segregation.

Low gravity processing eliminates Stokes forces that dominate the segregation processes for large (> 1 micron) particles. This allows the study for control of normally masked surface energy driven processes. Small particles suspensions (< 1 micron, Brownian collisions dominate aggregation) can be solidified without buoyancy driven convective flows. Low-gravity experimental results can be used to modify ground processing for improved properties, to develop space construction processes (e. g. welding of oxide strengthened composites in space), or for production of unique space processed materials.

The first low gravity ceramic metal matrix composite experiments were first performed on Skylab. (For a review of low gravity results for composite processing see Walter, 1987.) Gravity driven segregation of SiC whiskers in Ag decreased yielding a composite with improved (relative to normal gravity processing) mechanical properties. These results were confirmed with low gravity sounding rocket experiments. Solidification of metal matrix composite with large (1 - 160 micron) ceramic particles also have yielded more homogeneous dispersions in low gravity. Surface tension driven segregation and effects of grain boundaries can dominate segregation in low gravity. Composites with small (0.1 - 0.5 micron) oxide particles solidified with a more homogeneous dispersion and with less particle free areas in low gravity. Since, Stokes forces (sedimentation and flotation) are not strong for this size particles, the improved homogeneity was hypothesized due to lack of convective flows.

Morphological Stability of the Solid/Liquid Interface

The solute composition at the solid/melt interface is dependent on convective flow. Thus, convection by stagnant film arguments will influence the constitutional supercooling criterion for solid/liquid interfacial morphological stability. More detailed analysis show that it is critical to consider both thermal and solutal convective flow. Numerically analysis (13) has been reported for coupled thermosolutal convection and morphological stability for Pb-Sn alloy solidified in the vertical stabilized Bridgman configuration. The calculated stability diagram for thermosolutal convective flow is given in Figure 12.

Morphological Stability in Low Gravity. The influence of gravity on the planar to cellular transition for iron-carbon-silicon-phosphorous alloy has been examined by directional solidification during multiple aircraft parabolic low-gravity maneuvers. Sample composition, gradient, and growth rate were selected such that the interface was only marginally morphologically stable during solidification in one-gravity. Samples were then solidified under the same conditions except during low-gravity maneuvers (continuous cycling of about 25 sec

at .01 g and 1 minute at 1.8 g). The solid-liquid interface became more unstable in low gravity and could be made to shift from planar to cellular type solidification morphology during the shift in aircraft gravity form 1.8 to 0.01 g (Figure 13). Al-Cu solidified in Space found greater destabilization also for Al-1%Cu interface in low-gravity (14).

Cellular Growth in Low Gravity. Eutectic cell (eutectic grain) size for austenite-flake graphite eutectic (Fe-C-Si-P) has been shown to increase in low gravity during directional solidification in aircraft low gravity maneuvers (4). The cell diameter for nickel base superalloy (relative to one-gravity control samples) was two times greater (15) for low gravity solidification on Spacelab.

Gravity's Influence on Dendritic Solidification and Casting

Dendritic growth processes are critical to the most common alloy casting techniques. Dendrite arm spacings correlate with mechanical strength. Interdendritic macrosegregation causes non-homogeneous casting properties; yet, controlled segregation is utilized for precipitation strengthening processes. Buoyancy-driven convective flow in the liquid perturbs metal alloy solute concentration profiles (and to a lesser degree temperature profiles) that control microstructure and properties. Gravity, thus, has strong influence on the processes of dendritic growth.

Dendrite Tip Growth Morphology and Growth Velocity. Single dendrites of pure succinonitrile have been studied (16) as a function of undercooling, tip growth rate, and orientation to gravity. Gravity-independent diffusion-limited growth occurs at undercooling of 1 to 9 C. Morphology (Figure 14) and growth rate are dependent, however, at undercoolings less than 1 C on dendritic orientation to gravity. The growth rate perturbations observed at small undercooling are consistent with enhanced transfer of latent heat by natural convection. Low-gravity experiments (14) with Al-0.4Cu show that convection can influence dendritic morphology and crystallographic orientation in metallic alloys.

Gravity and Dendritic Spacing. Table II lists the results of low-gravity solidification studies on dendrite spacings (17). The effect of low gravity on secondary dendrite spacings was studied on sounding rockets (5 min at 0.0001 g) for ammonium chloride/water metal-model material and for Pb-Sn binary alloy, and on parabolic aircraft maneuvers for iron-carbon and MAR-M246 superalloy. Primary dendrite spacings have been studied by solidification on orbital laboratories for Al-Cu (Figure 15) and during parabolic aircraft maneuvers for iron-carbon and PWA-1480 superalloy (Figure 16). In all studies to date, in which a difference has been noted, regardless of alloy complexity low-gravity solidification (relative to solidification in normal gravity) results in coarser dendritic spacing.

(a) Local Solidification Time

Local solidification times, t_f for Al-Cu and Nimonic-90 (Co-Ni) alloys have been found (17) to decrease with increasing forced convective flow velocity. Forced convection also decreased primary dendrite spacing. Al-Cu secondary dendrite spacings have previously been observed (17) also to decrease with decreasing t_f.

Convection influences t_f by improving mold-metal heat extraction and by increasing solute transfer. The behavior of local solidification time in low-gravity dendritic solidification remains to be established. Continued increase in t_f with the elimination of natural convection in low gravity would increase dendrite spacings.

(b) Buoyancy-Driven Interdendritic Solute Transport

Primary dendrite spacing difference of a factor of 10 has been noted (17) between ammonium chloride/water metal-model grown parallel (down) and that grown anti-parallel (up) to gravity. Ammonium chloride freezes dendritically analogous to primary metal. Water (analogous to the alloying element) is the rejected solute. It is believed that the spacing difference is due to buoyancy-driven fluid flow. For upward growth, less dense rejected solute (water rich) is driven from the interdendritic region by buoyancy-driven flow. For downward growth the solute density gradient is convectively stable (similar to conditions in low gravity); solute transport and therefore dendrite spacing is limited by diffusion.

The influence of gravity on solute transport, and thus, interdendritic constitutional supercooling, can explain the adjustment of primary spacing to gravity level for superalloy (Figure 16 and 17) during solidification through multiple aircraft parabolas. Buoyancy-driven flow is expected to increase interdendritic solute transport. This is consistent with available low-gravity data (Table II) in which all tested alloy types result in unchanged or increased primary spacing.

(c) Dendrite Arm Coarsening in Low Gravity

The expected effect of low gravity on coarsening rate is dependent on the coarsening mechanism. Zero gravity eliminates convective transport of interdendritic rejected solute. Increased average solute concentration reduces dendrite curvature and therefore reduces dendrite coarsening by the arm coalescence model. However, thinning dendrite arms will cause increased coarsening with increased solute concentration for the arm-melting model.

Dendrite arm coarsening for Al-Cu alloy has been measured (20) by interface quenching experiments in an orbital low-gravity laboratory. Initial results show lower dendrite coarsening rate in low gravity. This indicates (confirming earlier suggestions, 17) that dendrite arm coarsening for Al-Cu is primarily by

coalescence.

Interdendritic Fluid Flow - Macrosegregation. Thermal solutal convection and solidification shrinkage produce interdendritic fluid flow that is directly related to casting macrosegregation and porosity. Interdendritic flow perturbs concentration and temperature fields that determine local solid composition in the casting. Al-Cu dendritic solidification perpendicular to the gravity vector has been analyzed as a function of magnitude of gravity. Macrosegregation under normal gravity causes Cu fraction across the casting to vary 45%. Since flow due to solidification shrinkage is perpendicular to the thermal isotherms, theory predicts (21) negligible macrosegregation in zero gravity. Low-gravity dendritic directional solidification (17) of off-eutectic Pb-Sb, Bi/Mn-Bi, Al-Cu (Figure 17), and Sn-Pb have resulted in negligible macrosegregation indicating diffusive solute transport.

Dendritic Macroscopic Solid/Liquid Interface Shape. Dendritic solidification of off-eutectic alloy in the convectively stable configuration (the solid and denser liquid down) minimizes buoyancy-driven macrosegregation. This configuration, however, (except for compositions where thermal and solutal buoyancy forces balance) produces interfacial "steepling" and "dendritic clustering" (22) casting defects. The denser solute rich liquid settles into solid/liquid interfacial depressions. The increase in solute concentration causes the depressions to deepen. The interfacial curvature increasingly exceeds the curvature of the isotherm producing interfacial steepling. Thus, for dendritic directional solidification, the convectively unstable configuration results in macrosegregation, and the convectively stable configuration results in solid/liquid interface steepling producing dendritic clustering in the solidified casting.

Channel-Type Segregates ("Freckle" Casting Defects). Ingots of commercial alloys often contain defects consisting of vertical solute rich lines of refined grain structure termed channel type segregates or "freckles." Superalloy and transparent model studies (17) have demonstrated that this casting defect results from interdendritic thermal solutal convective flow. The process has recently been modeled with quantitative agreement to experiment. When interdendritic flow solutally enriches a particular mushy zone area, local dendritic remelting occurs. The increased interdendritic channel size results in decreased resistance to flow and further remelting. This process results in local solute enrichment on the order of 30%. Debris of remelted dendrites act as nuclei refining the channel grain structure. In low gravity the elimination of thermosolutal convective flow removes the driving force force for channel type segregate formation.

Grain Multiplication and Casting Grain Structure. At the chill surface of a casting (in the absence of nucleation agents) convection is a primary cause of grain multiplication. Conversely, chill zone formation in castings can be prevented

(17) by damping convective flow. Transparent model studies show that convective pulses at the dendrite roots cause dendrite remelting. Dendrite fragments are swept from the solid/liquid interface by the convective flow which simultaneously dissipates superheat. The fragments nucleate new grains that grow in the equiaxed region of the casting. Experiments with metal alloys and with model materials (Figures 19 and 20) show that the grain refinement by this mechanism increases under forced convection; conversely it is absent in low gravity.

Table I

Effect of Low Gravity for On-Eutectic Interphase Spacing
(Various Authors)

Alloy Composition	Low-Gravity Solidification Effect on Interphase Spacing
Lamellar Eutectics	
Al_2Cu/Al	no change
Fe_3C/Fe	- 25 %
Fibrous Eutectics	
MnBi/Bi	- 50 %
InSb/NiSb	- 20 %
Al_3Ni/Al	+ 17 %

Table II

The Effect of Low Gravity on Dendrite Spacing
(Various Authors)

Composition	$g - g_{low}$	Low-Gravity Solidification Relative Dendrite Spacings
NH_4Cl-H_2O	1 - 0.0001	+30% Sec., +10% Tert.
Al-Cu	1 - 0.00001	+150% Prim.
Pb-Sn	1 - 0.0001	+50% Sec.
MAR-M246	1.8 - 0.01	+50% Sec.
Fe-C-Si-P	1.8 - 0.01	+20% Sec.
PWA-1480	1.8 - 0.01	+20% Prim.
Al-Cu	1 - 0.001	+500% Prim.

REFERENCES

1. F. Rosenberger and G. Muller, Journal of Crystal Growth 65 (1983) 102.

2. C. J. Chang and R. A. Brown, Journal of Crystal Growth 63 (1983) 350.

3. M. H. Johnston and R. B. Owen, Metallurgical Transactions 14A (1983) 2164.

4. D. M. Stefanescu, P. A. Curreri, and M. R. Fiske, Metallurgical Transactions, 17A (1986) 1121-1130.

5. D. J. Larson and R. G. Pirich, "Influence of Gravity Driven Convection on the Directional Solidification of Bi/MnBi Eutectic Composites," Materials Processing in the Reduced Gravity Environment of Space, ed. G. E. Rindone (Materials Research Society, Pittsburgh, PA, 1982) 523-532.

6. R. G. Pirich, Space Processing Applications Rocket (SPAR) Project, SPAR IX, Final Report (NASA Technical Memorandum 82549, 1984) III, 1-46.

7. P. A. Curreri, D. J. Larson, and D. M. Stefanescu, "Influence of Convection on Eutectic Morphology," Solidification Processing of Eutectic Alloys, Proceedings of the 1987 TMS Fall Meeting, to be published.

8. J. M. Quenisset and R. Naslain, Journal of Crystal Growth 54 (1981) 465-474.

9. V. Baskaran and W. R. Wilcox, Journal of Crystal Growth 67 (1984) 343-352.

10. L. L. Lacy and G. H. Otto, AIAA Journal 13 (1975) 219.

11. M. K. Wu, J. R. Ashburn, C. J. Torng, P. A. Curreri, and C. W. Chu, "Pressure Dependence of the Electrical Properties of GaBi Solidified in Low Gravity," Materials Processing in the Reduced Gravity Environment of Space, vol. 87, eds. R. H. Doremus and P. C. Nordine (North-Holland, N. Y., 1987) pp. 77-84.

12. M. K. Wu, J. R. Ashburn, P. A. Curreri, and W. F. Kaukler, Metallurgical Transactions 18A (1987) 1515.

13. S. R. Coriell, M. R. Cordes, W. J. Boettinger, and R. F. Sekerka, Journal of Crystal Growth 49 (1980) 22.

14. J. J. Favier, J. Berthier, Ph. Arragon, Y. Malmejac, V. T. Khryapov, and I. V. Barmin, Acta Astronautica, 9 (1982) 255-259.

15 H. J. Sprenger, "Skin Technology - Directional

Solidification of Multiphase Alloys," Scientific Results of the German Spacelab Mission D1, ed. P. R. Sham, R. Jansen, and M. H. Keller (DFVLR, Germany, 1987), chapter 7, 46-59.

16. M. E. Glicksman, N. B. Singh, and M. Chopra, "Influence of Diffusion and Convective Transport on Dendritic Growth in Dilute Alloys," Materials Processing in the Reduced Gravity Environment of Space, ed. G. E. Rindone (Materials Research Society, Pittsburgh, PA, 1982) 523-532.

17 P. A. Curreri, J. E. Lee, and D. M. Stefanescu, "Dendritic Solidification of Alloys in Low Gravity," Proceedings of the Second International Symposium on Experimental Methods for Microgravity Materials Research, 117th TMS-AIME Annual Meeting, 1988, to be published.

18 D. Camel, J. J. Favier, M. D. Dupouy, and R. le Maguet, "Microgravity and Low-Rate Dendritic Solidification," Scientific Results of the German Spacelab Mission D1, ed. P. R. Sham, R. Jansen, and M. H. Keller (DFVLR, Germany, 1987), chapter 4, 25-35.

19 M. H. McCay, J. E. Lee, and P. A. Curreri, Metallurgical Transactions 17A (1986) 2301-2303.

20. H. M. Tensi and J. J. Schmidt, "Influence of Thermal Gravitational Convectional on Solidification Processes," Scientific Results of the German Spacelab Mission D1, ed. P. R. Sham, R. Jansen, and M. H. Keller (DFVLR, Germany, 1987), chapter 4, 5.

21 A. L. Maples and D. R. Poirier, Metallurgical Transactions, 15B (1984) 163-172.

22 J. D. Verhoeven, J. T. Mason, and R. Trivedi, Metallurgical Transactions, 17A (1986) 991-1000.

23 M. H. Johnston and R. A. Parr, "Low-Gravity Solidification Structures in the Tin-15 WT % Lead and Tin-3 WT % Bismuth Alloys," Materials Processing in the Reduced Gravity Environment of Space, ed. G. E. Rindone (Materials Research Society, Pittsburgh, PA, 1982) 651-656.

SELECTED REFERENCES

R. J. Naumann and H. W. Herring, Materials Processing in Space: Early Experiments, (1980) NASA SP-443.

Proceedings of the Third Space Processing Symposium Skylab Results: Volume I, (NASA Report Number M-74-5, 1974).

H. U. Walter, Fluid Sciences and Material Sciences in Space (Springer-Verlag, New York, 1987).

FIGURE CAPTIONS

Figure 1 Schematic of the sensitivity of the temperature field to fluid flow for a melts with high and low Pr. (a) Pr >> 1. (b) Pr << 1. Dashed line represent temperature profile from thermal conduction only. Light line is convective velocity and heavy line is the corresponding temperature profile. (Ref. 1)

Figure 2 Laser interferograms of NH_4Cl/H_2O transparent model during initial solidification upwards in normal gravity showing the development of solutal convective plumes.

Figure 3 Transverse section of Bi/MnBi rod eutectic solidified in low gravity (SPAR IX sounding rocket) and a one-gravity control sample. (Ref. 5)

Figure 4 Intrinsic magnetic coercivity as a function of heat treatment for Bi/MnBi eutectic solidified in one gravity and in low gravity. (Ref. 6)

Figure 5 Interrod spacing for Bi/MnBi versus velocity for samples solidified parallel and antiparallel to gravity on earth and for low gravity solidified samples. (Ref. 6)

Figure 6 Predicted evolution of undercooling-interphase spacing with forced convective flow parallel to the solid-liquid interface from the Quenisset-Naslain model (Ref. 8).

Figure 7 Solidification temperature (undercooling) data for MnBi/Bi solidified in low gravity relative to one-gravity controls (Ref. 6).

Figure 8 Photomicrographs of Ga-Bi hypermonotectic alloy samples solidified under identical conditions except gravity. (Ref. 10)

Figure 9 Temperature dependence of the resistance of GaBi hypermonotectic samples solidified in one gravity (GC) and during free fall (DT, 10^{-4} g). (Ref. 11)

Figure 10 Superconducting transition temperature, T_c, for GaBi hypermonotectic samples showing higher T_c phase in low-gravity sample. (Ref. 11)

Figure 11 Superconducting transition temperature, resistivity ratio, and gravitational acceleration during solidification for Al-In-Sn monotectic sample solidified during KC-135 aircraft low gravity maneuvers. (Ref. 13)

Figure 12 Calculated stability diagram for critical concentration of Sn versus solidification velocity for PbSn (grown in the vertical stabilized Bridgman configuration). Curves are the composition above which thermosolutal convection instability occurs. Lower line is the neutral density criterion. Upper line represents the morphological instability criterion.

(Ref. 13)

Figure 13 Transition from planar (type A graphite) to cellular solidification (independent nucleation type D graphite and eutectic grains) at a high-gravity to low-gravity transition. (Magnification 46 times). (ref. 4)

Figure 14 Influence of orientation to gravity on dendritic morphology showing suppression of side-branches for inclinations above 90 degrees to gravity. (Ref. 16)

Figure 15 Transverse sections of Al- 26Cu alloy grown vertically in one gravity (a) and in orbit on Spacelab (b). The dendrites in the low-gravity solidified sample have coarser more regularly spaced dendrites and negligible radial segregation. (Ref. 18)

Figure 16 Average primary dendrite spacing versus solidification distance for PWA-1480 nickel base superalloy directionally solidified through multiple low-gravity maneuvers. (Ref. 19)

Figure 17 Mechanism for decreasing primary dendrite spacing during directional solidification during low-gravity to high-gravity portion of aircraft parabolas. (a) Dendritic growth in low gravity. Solute transport is by diffusion. (b) Dendritic growth continues in high gravity. Solute transport is increased by buoyancy-driven convection. Interdendritic constitutional supercooling increases. (c) Ternary arm driven by increased constitutional supercooling grows to the dendrite tip growth front decreasing interdendritic spacing. (Ref. 17)

Figure 18 Copper concentration versus distance for directionally solidified Al-Cu samples showing decreased macrosegregation for the low-gravity solidified sample. (Ref. 14)

Figure 19 NH_4Cl-H_2O transparent model solidified in one gravity and in low gravity. (Ref. 23)

Figure 20 Sn-15Pb sample solidified at high gravity in a centrifuge and in low-gravity showing illustration grain refinement at higher gravity. (Ref. 23)

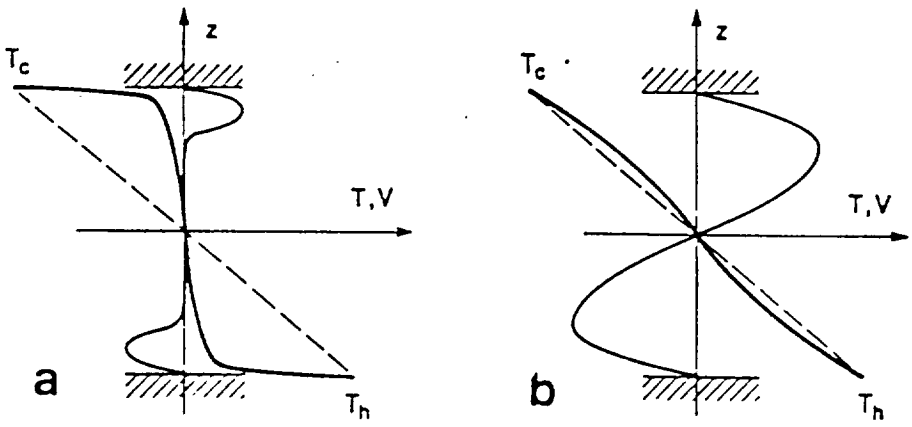

Fig. 1

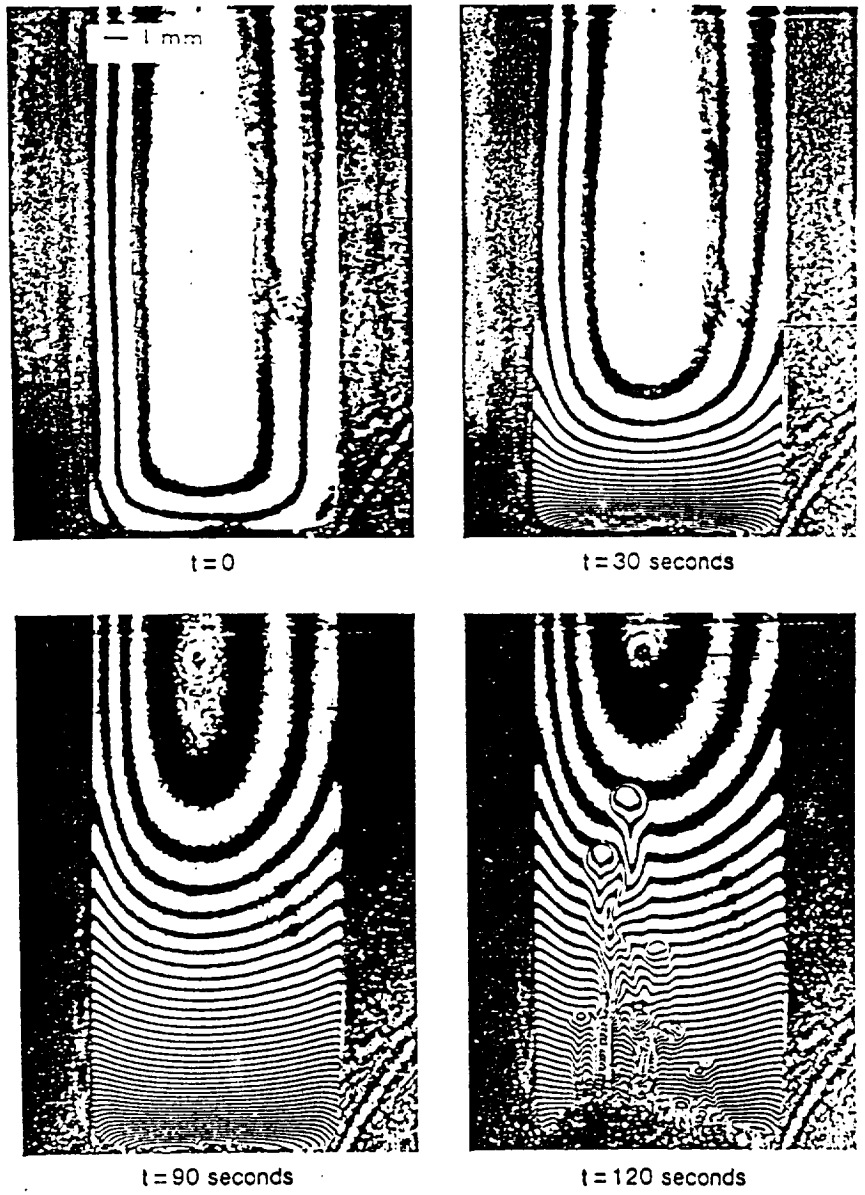

Fig. 2

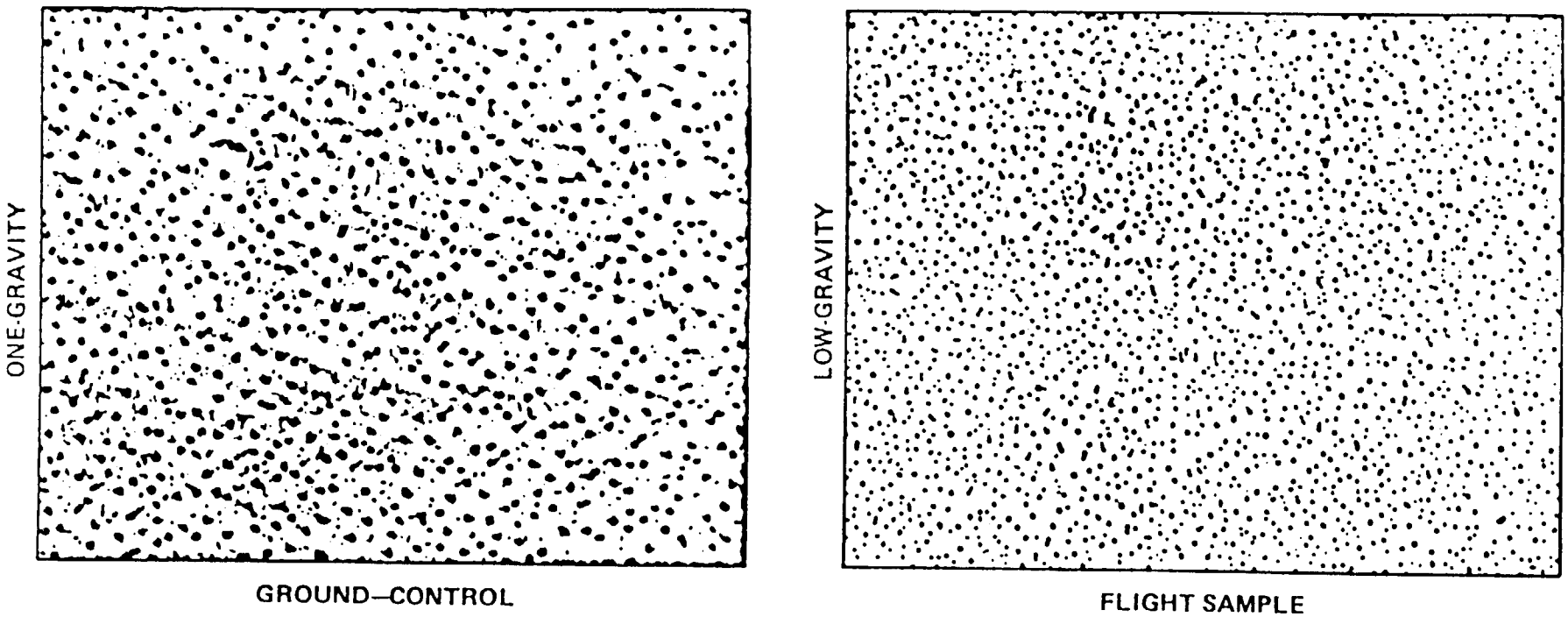

Fig. 3

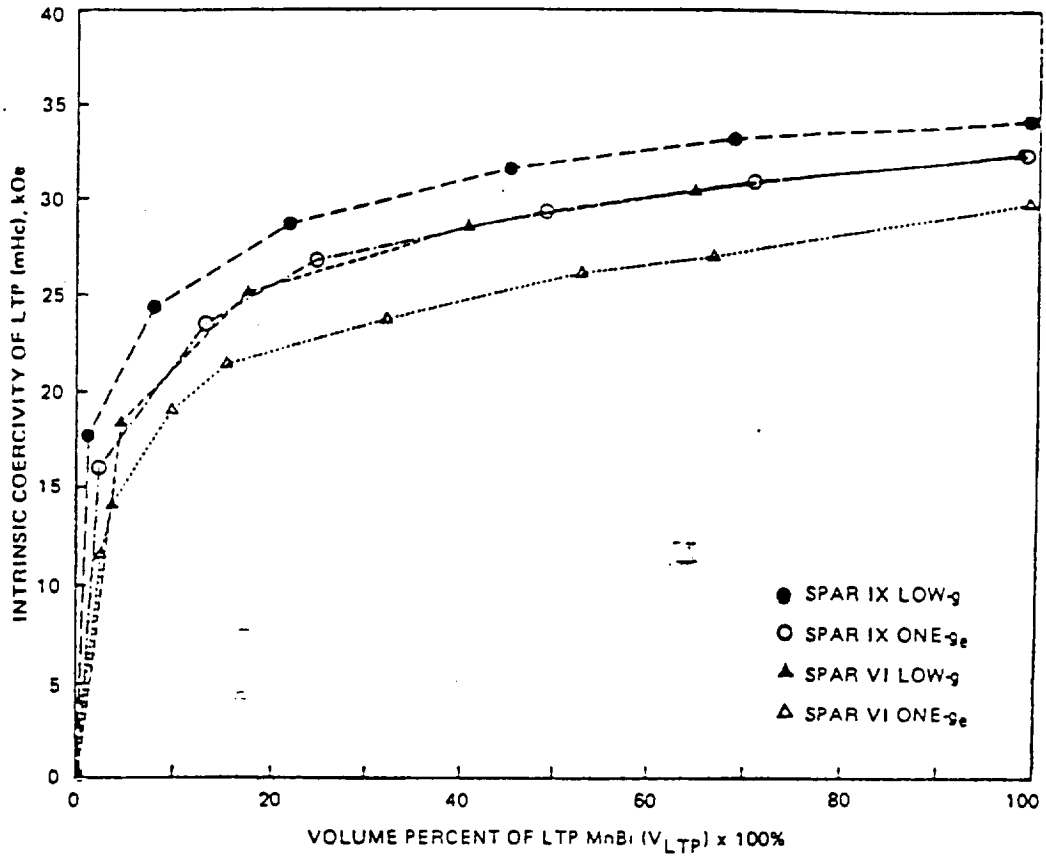
INTRINSIC COERCIVITY OF LTP (mHc), kOe
VOLUME PERCENT OF LTP MnBi (V_{LTP}) x 100%
SPAR IX LOW-g
SPAR IX ONE-ge
SPAR VI LOW-g
SPAR VI ONE-ge
0
5
10
15
20
25
30
35
40
0
20
40
60
80
100

Fig. 4

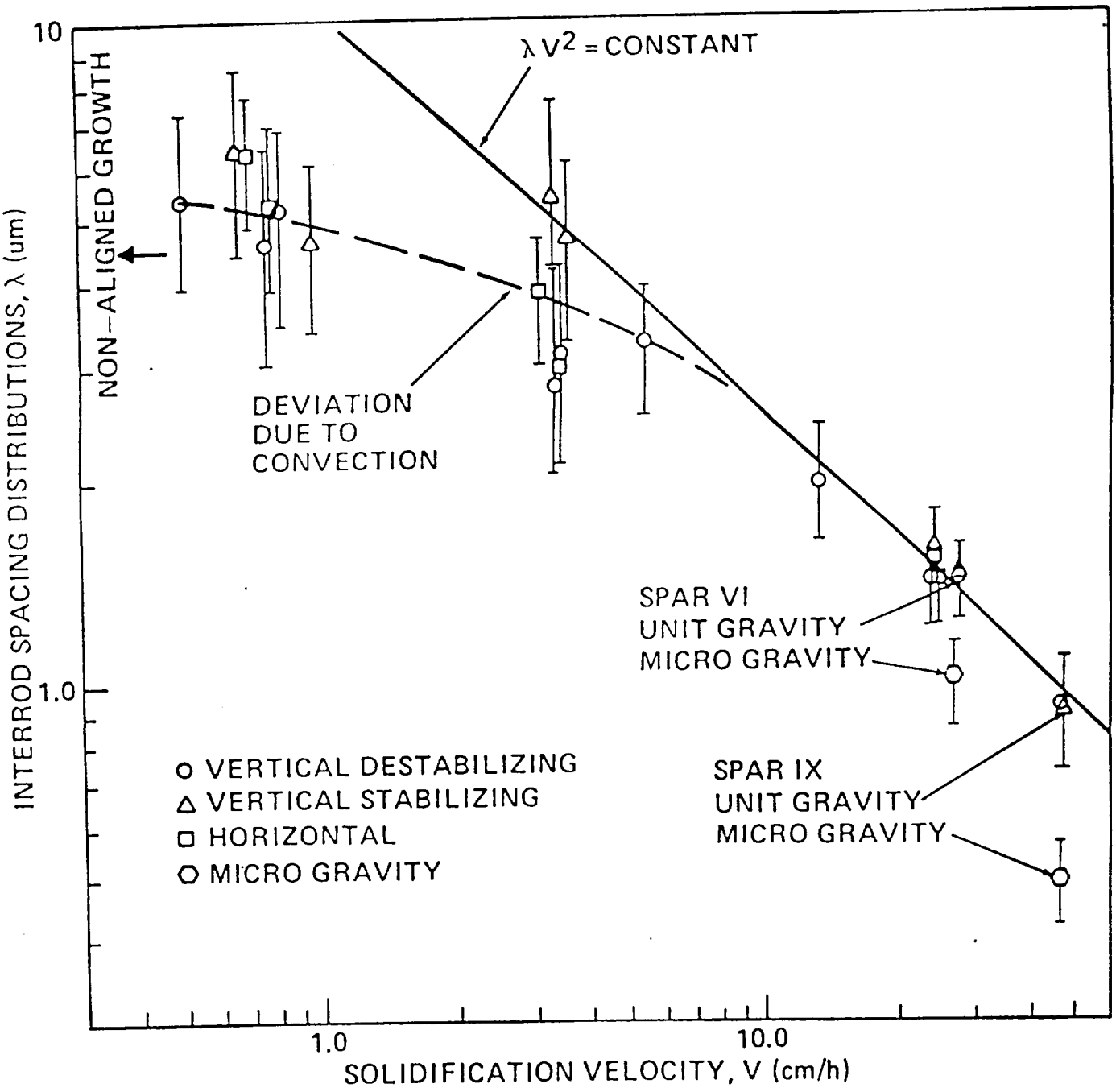
10
1.0
INTERROD SPACING DISTRIBUTIONS, λ (um)
λ V² = CONSTANT
NON-ALIGNED GROWTH
DEVIATION
DUE TO
CONVECTION
SPAR VI
UNIT GRAVITY
MICRO GRAVITY
SPAR IX
UNIT GRAVITY
MICRO GRAVITY
VERTICAL DESTABILIZING
VERTICAL STABILIZING
HORIZONTAL
MICRO GRAVITY
1.0
10.0
SOLIDIFICATION VELOCITY, V (cm/h)

Fig. 5

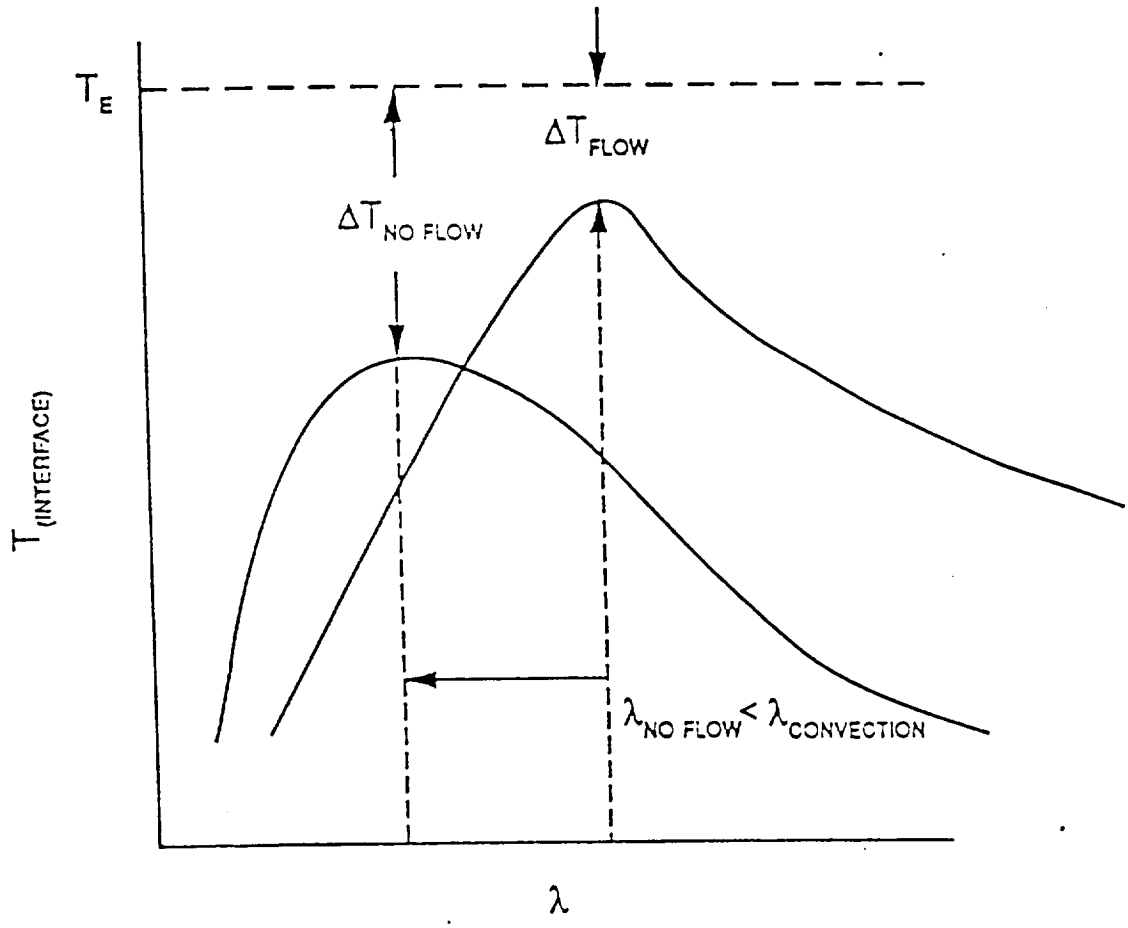
T_E
ΔT_{FLOW}
$\Delta T_{NO\ FLOW}$
$T_{(INTERFACE)}$
$\lambda_{NO\ FLOW} < \lambda_{CONVECTION}$
λ

Fig. 6

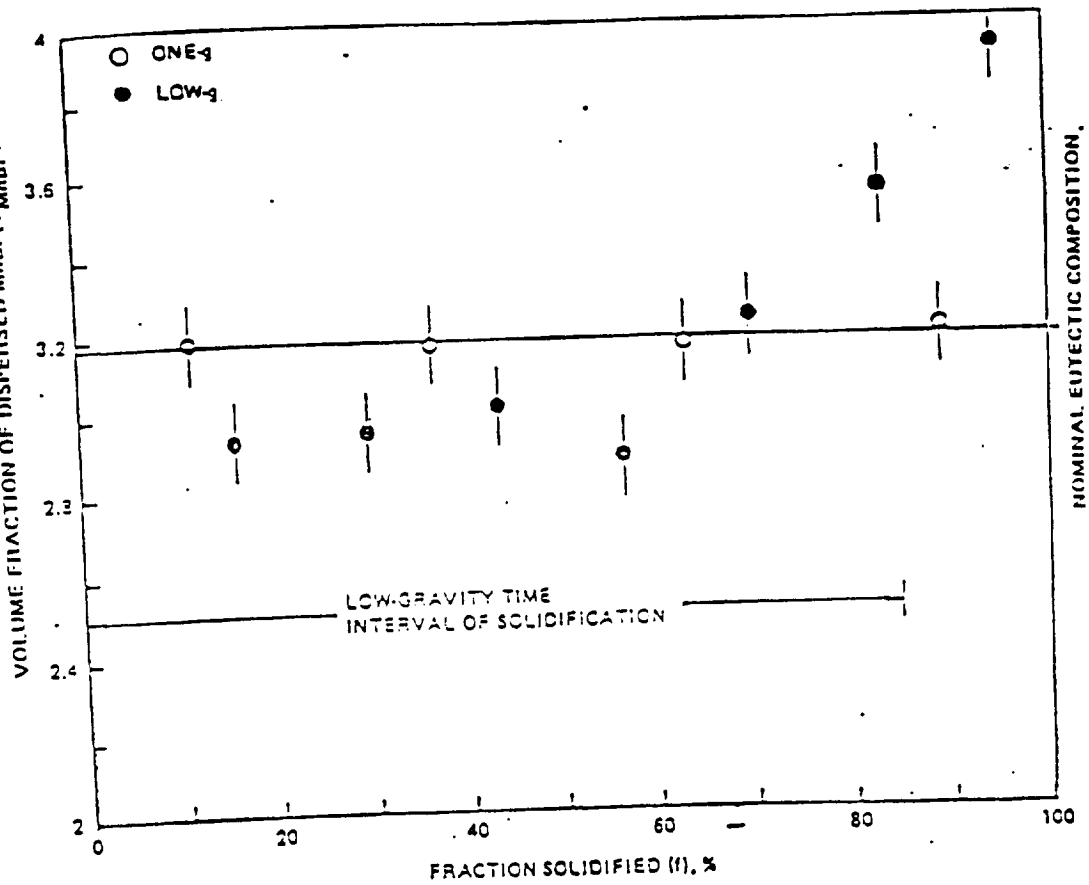
ONE-g
LOW-g
VOLUME FRACTION OF DISPERSED MnBi (V_{MnBi}), %
NOMINAL EUTECTIC COMPOSITION,
LOW-GRAVITY TIME
INTERVAL OF SOLIDIFICATION
FRACTION SOLIDIFIED (f), %
4
3.6
3.2
2.8
2.4
2
0
20
40
60
80
100

Fig. 7

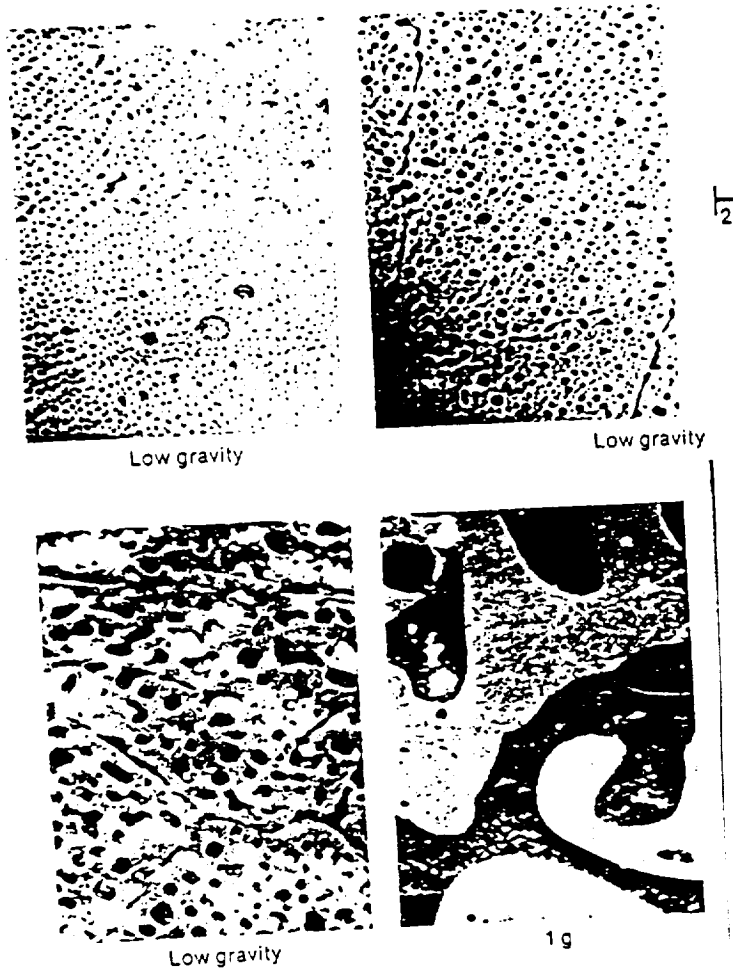

Fig. 8

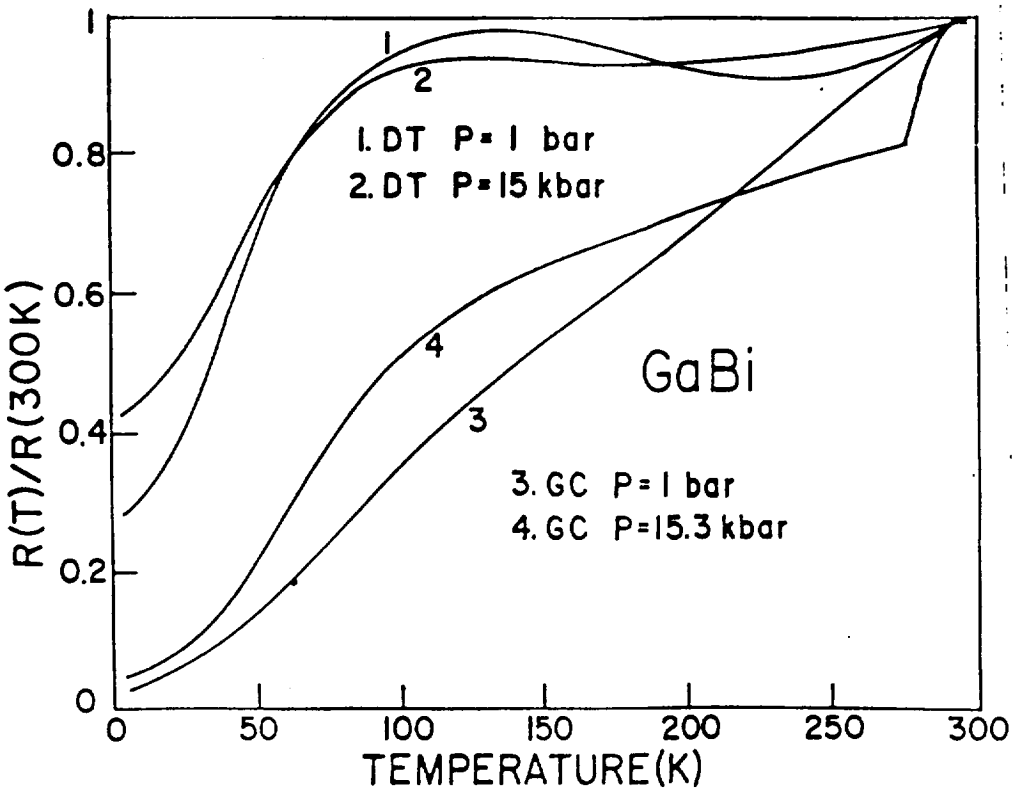
1
0.8
0.6
0.4
0.2
0
R(T)/R(300K)
0
50
100
150
200
250
300
TEMPERATURE(K)
1. DT P = 1 bar
2. DT P = 15 kbar
3. GC P = 1 bar
4. GC P = 15.3 kbar
GaBi
1
2
3
4

Fig. 9

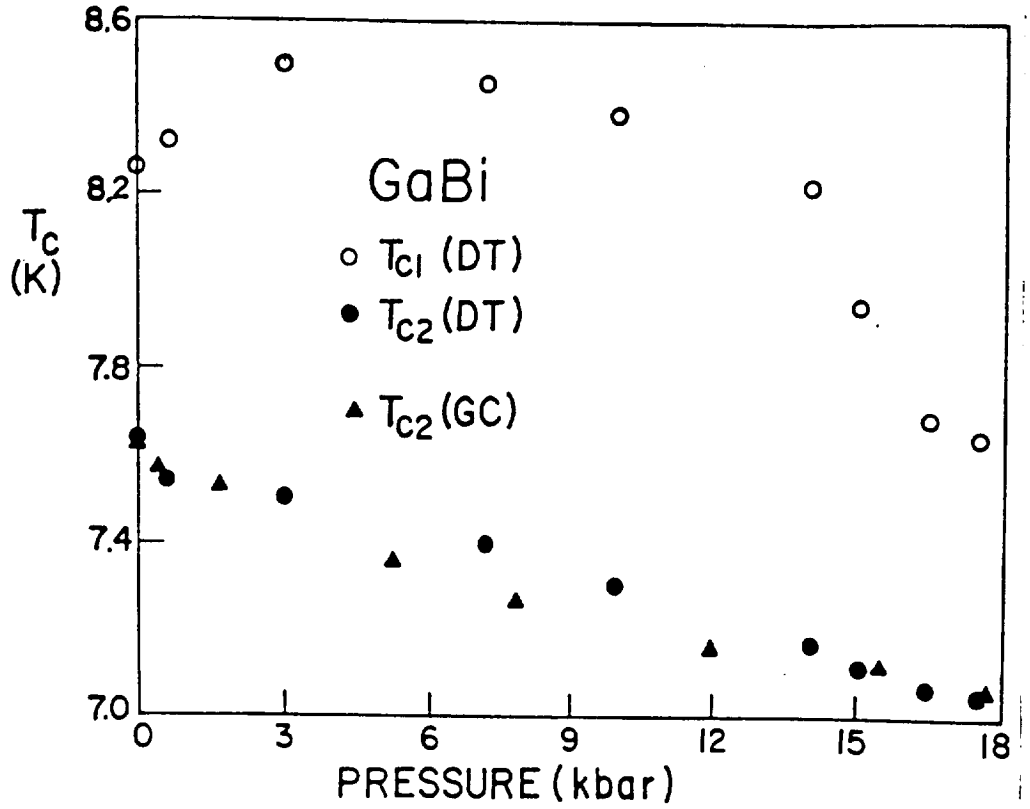
8.6
8.2
7.8
7.4
7.0
T_c (K)
GaBi
T_{c1} (DT)
T_{c2} (DT)
T_{c2} (GC)
0
3
6
9
12
15
18
PRESSURE (kbar)

Fig. 10

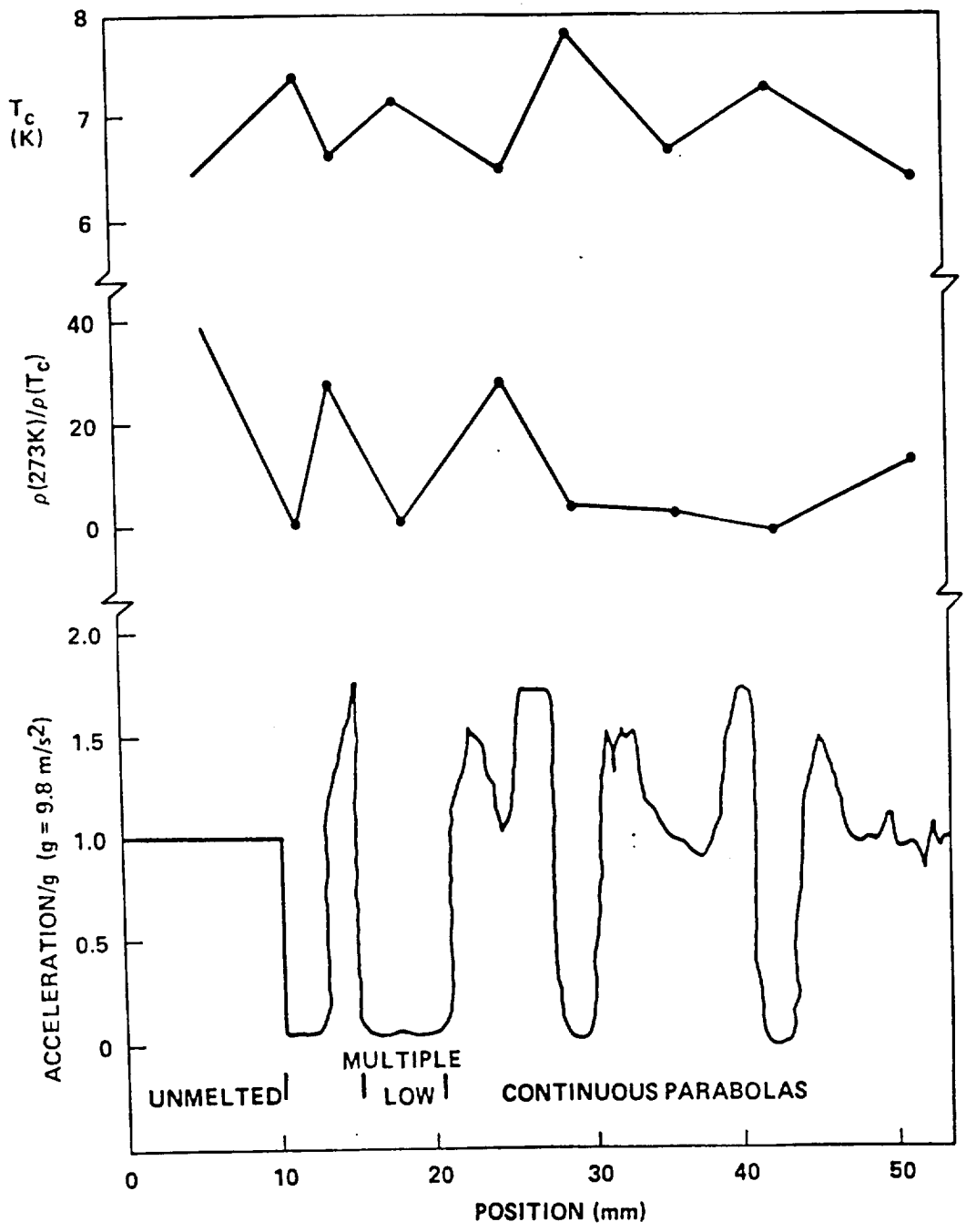
8
7
6
T_c (K)
40
20
0
$\rho(273K)/\rho(T_c)$
2.0
1.5
1.0
0.5
0
ACCELERATION/g (g = 9.8 m/s^2)
UNMELTED
MULTIPLE LOW
CONTINUOUS PARABOLAS
0
10
20
30
40
50
POSITION (mm)

Fig. 11

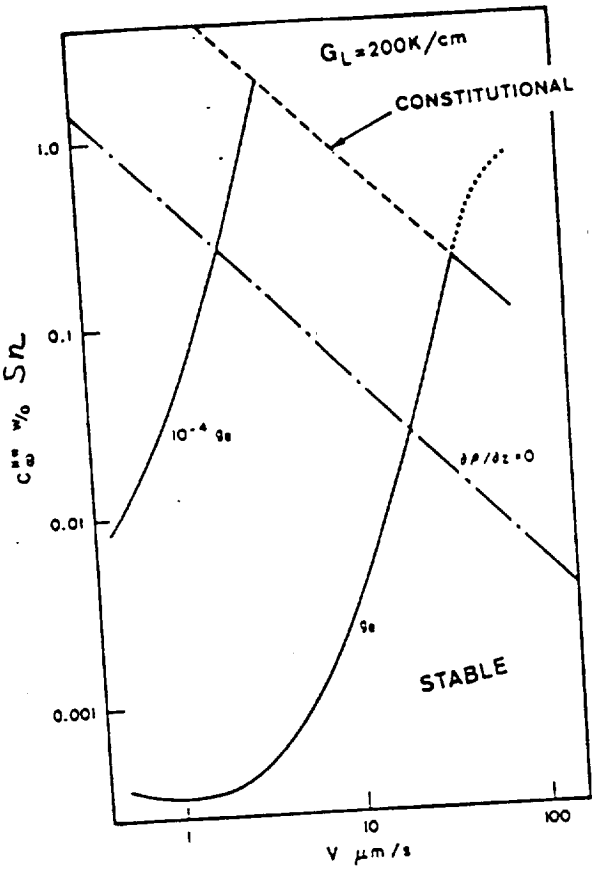
G_L=200K/cm
CONSTITUTIONAL
1.0
0.1
0.01
0.001
C_∞^{Sn} w/o Sn
10^{-4} g_e
$\partial P/\partial z = 0$
g_e
STABLE
1
10
100
V μm/s

Fig. 12

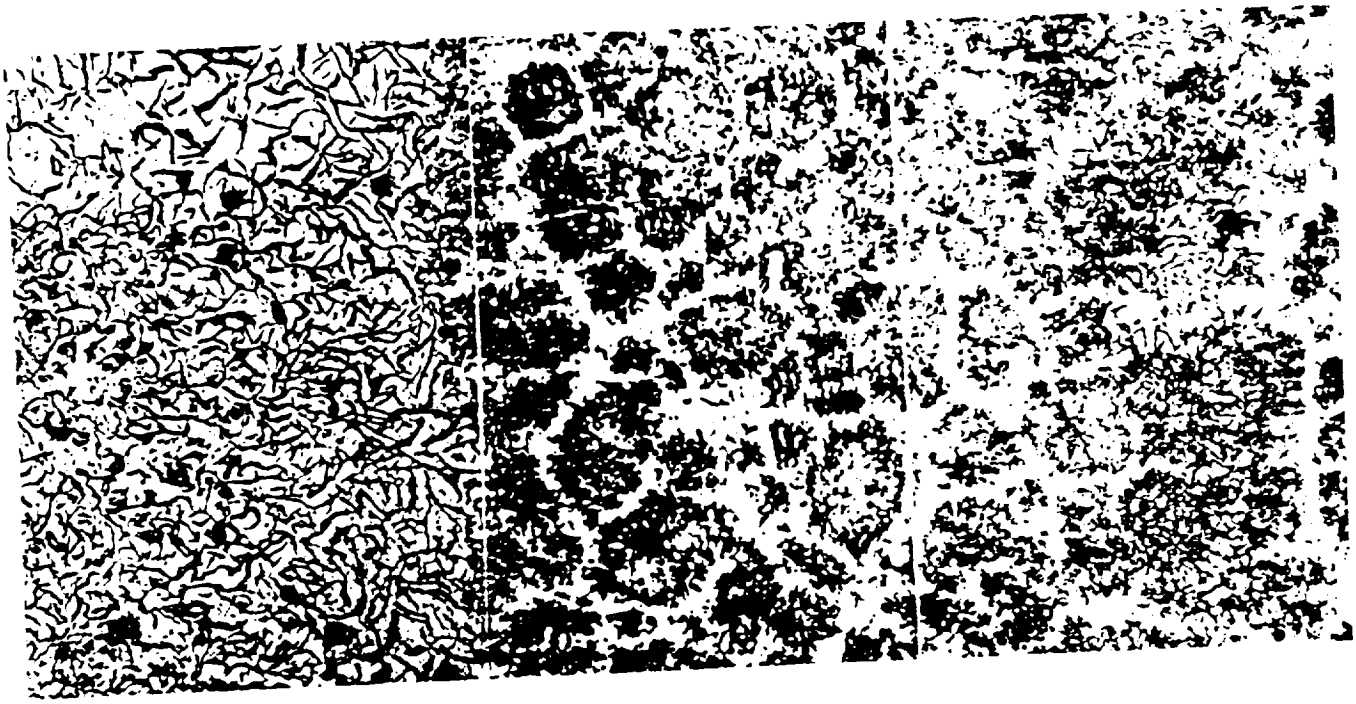

Fig. 13

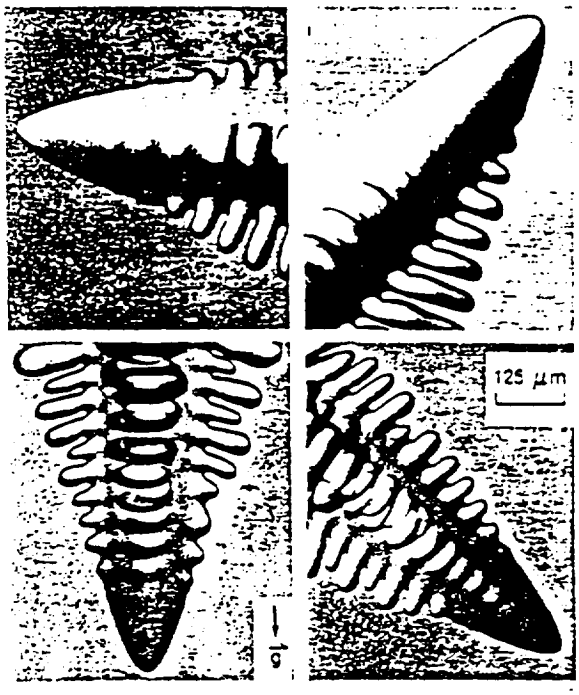

Fig. 14

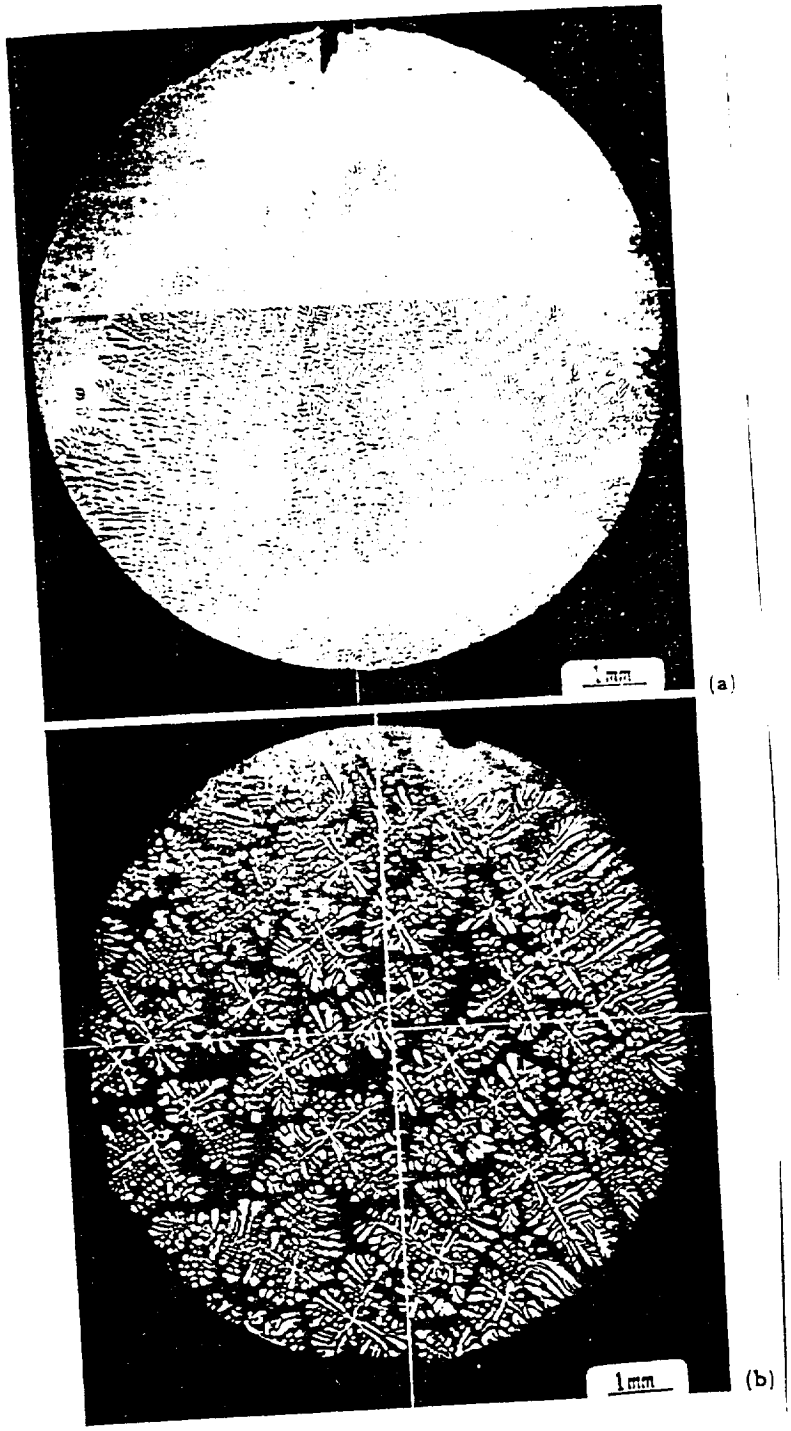

Fig. 15

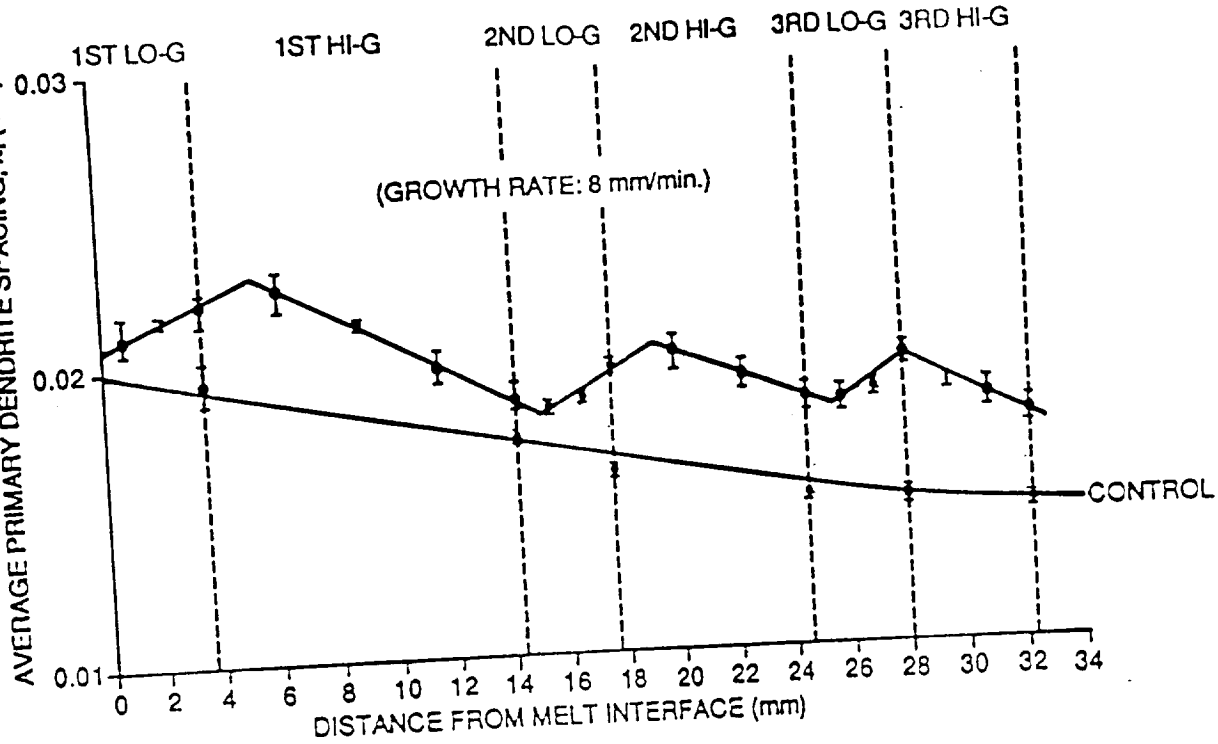
1ST LO-G
1ST HI-G
2ND LO-G
2ND HI-G
3RD LO-G
3RD HI-G
(GROWTH RATE: 8 mm/min.)
AVERAGE PRIMARY DENDRITE SPACING, $\bar{\lambda}$, (CM)
0.03
0.02
0.01
CONTROL
0 2 4 6 8 10 12 14 16 18 20 22 24 26 28 30 32 34
DISTANCE FROM MELT INTERFACE (mm)

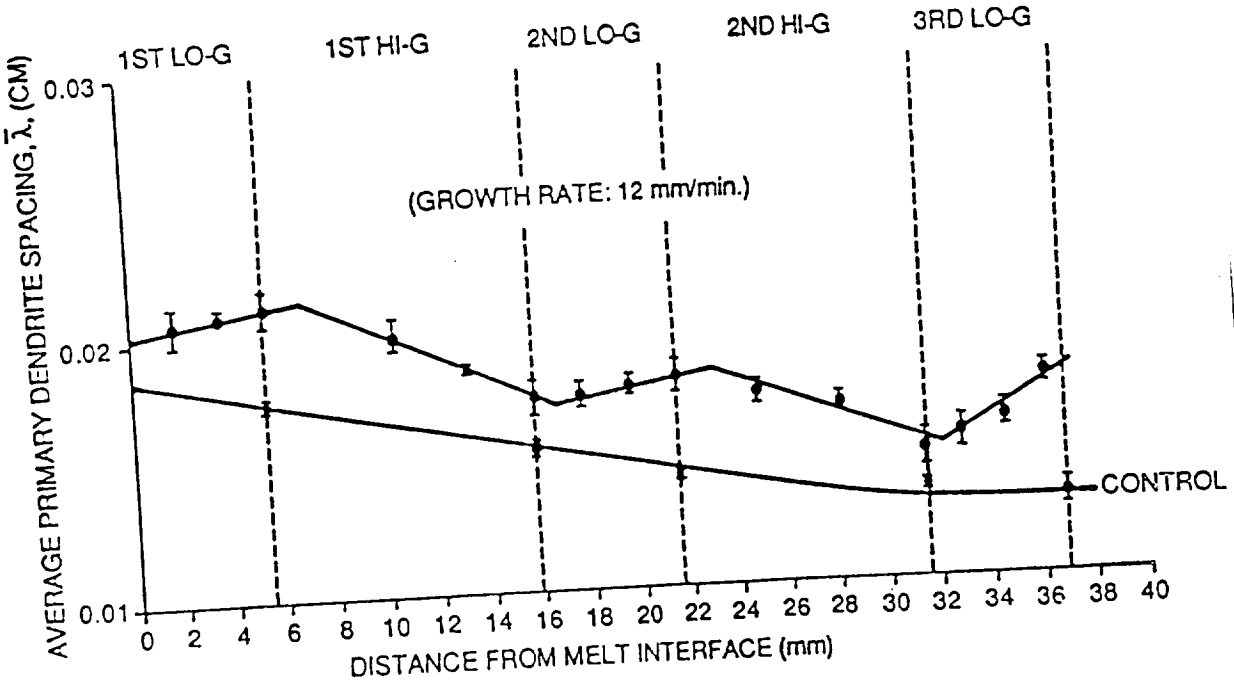
1ST LO-G
1ST HI-G
2ND LO-G
2ND HI-G
3RD LO-G
(GROWTH RATE: 12 mm/min.)
AVERAGE PRIMARY DENDRITE SPACING, $\bar{\lambda}$, (CM)
0.03
0.02
0.01
CONTROL
0 2 4 6 8 10 12 14 16 18 20 22 24 26 28 30 32 34 36 38 40
DISTANCE FROM MELT INTERFACE (mm)

Fig. 16

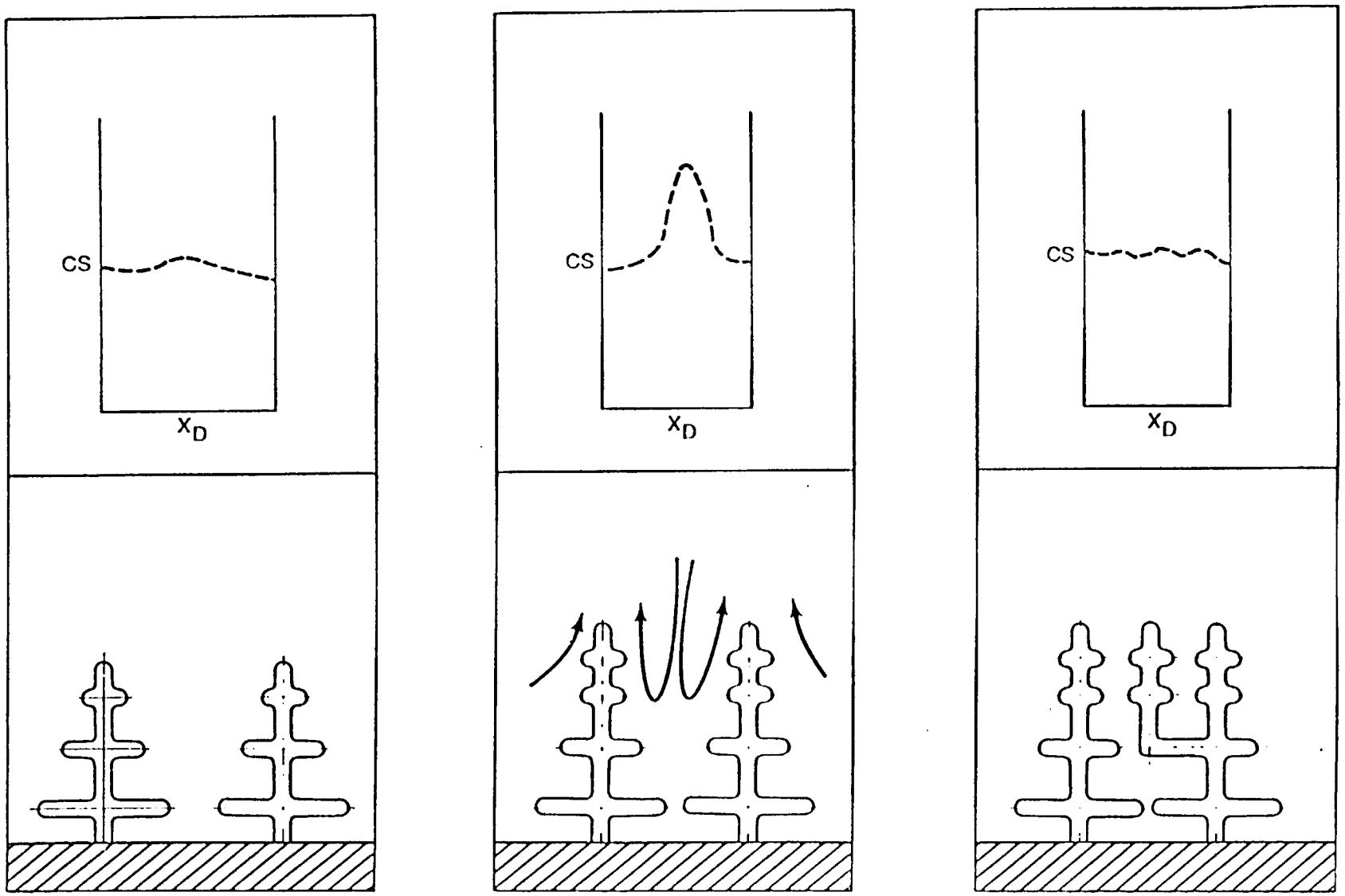

(A) LOW - GRAVITY

(B) HIGH - GRAVITY

(C) HIGH - GRAVITY

Fig. 17

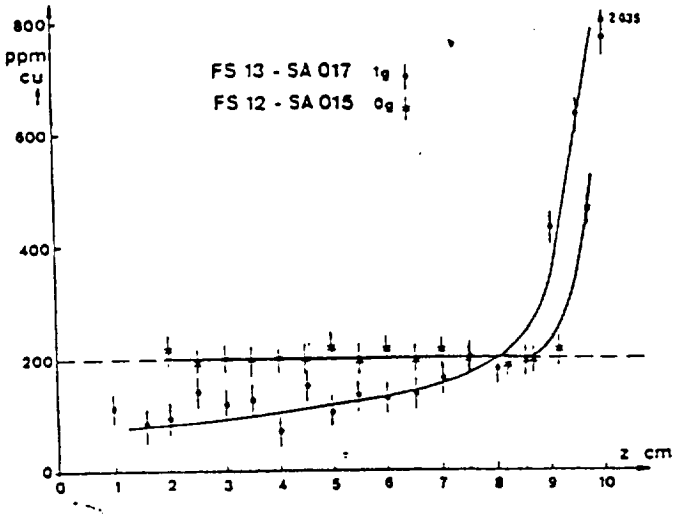

Fig. 18

One-Gravity

Low-Gravity

Fig. 19

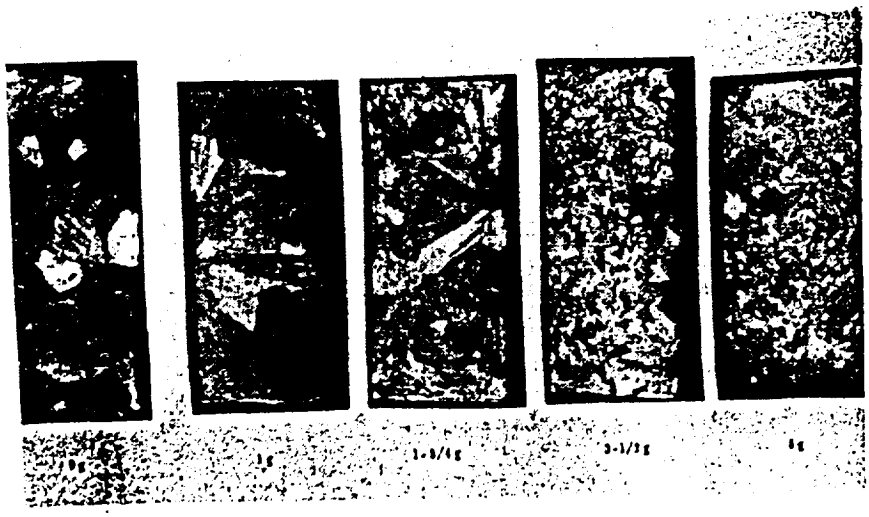

Fig. 20